

Photonic Crystal Cavities from Hexagonal Boron Nitride

Sejeong Kim^{1,#,*}, Johannes E. Fröch^{1,#}, Joe Christian², Marcus Straw², James Bishop¹, Daniel Totonjian¹, Kenji Watanabe³, Takashi Taniguchi³, Milos Toth^{1,*}, Igor Aharonovich^{1,*}

¹*Institute of Biomedical Materials and Devices (IBMD), Faculty of Science, University of Technology Sydney, Ultimo, NSW, 2007, Australia*

²*Thermo Fisher Scientific, 5350 NE Dawson Creek Drive, Hillsboro, OR 97214-5793 USA*

³*National Institute for Materials Science, 1-1 Namiki Tsukuba Ibaraki 305-0044 Japan*

*correspondence to Sejeong.Kim-1@uts.edu.au, milos.toth@uts.edu.au, igor.aharonovich@uts.edu.au

contributed equally to this work.

Abstract

Development of scalable quantum photonic technologies requires on-chip integration of components such as photonic crystal cavities and waveguides with nonclassical light sources. Recently, hexagonal boron nitride (hBN) has emerged as a promising platform for nanophotonics, following reports of hyperbolic phonon-polaritons and optically stable, ultra-bright quantum emitters. However, exploitation of hBN in scalable, on-chip nanophotonic circuits, quantum information processing and cavity quantum electrodynamics (QED) experiments requires robust techniques for the fabrication of monolithic optical resonators. In this letter, we design and engineer high quality photonic crystal cavities from hBN. We employ two approaches based on a focused ion beam method and a minimally-invasive electron beam induced etching (EBIE) technique to fabricate suspended two dimensional (2D) and one dimensional (1D) cavities with quality (Q) factors in excess of 2,000. Subsequently, we show deterministic, iterative tuning of individual cavities by direct-write, single-step EBIE without significant degradation of the Q -factor. The demonstration of tunable, high Q cavities made from hBN is an unprecedented advance in nanophotonics based on van der Waals materials. Our results and hBN processing methods open up promising new avenues for solid-state systems with applications in integrated quantum photonics, polaritonics and cavity QED experiments.

Main Text

Controlling and manipulating light at the nanoscale is important for a vast variety of applications that include sensing, quantum information processing, secure communications and cavity QED experiments¹⁻¹¹. Key components for most of these applications include optical resonators such as photonic crystal cavities, and non-classical light sources that can emit single photons on demand such as color centers in solids¹², defects in carbon nanotubes (CNTs)¹³, single molecules¹⁴ and quantum dots¹⁵. Remarkable progress has been achieved over recent years to realize on-chip integrated quantum photonic circuits that employ various combinations of these systems. For example, in a monolithic approach where nanophotonic elements and a quantum light source are embedded in the same material, coupled systems have been implemented using diamond^{5, 11}, rare earth crystals⁴, and gallium arsenide¹⁶. Alternatively, hybrid systems, where an external source is positioned in close proximity to the photonic element made from a foreign material, have been

assembled from a broad range of materials such as CNTs¹⁷ and InAsP quantum dots (QDs)^{18, 19} integrated with silicon nitride components.

In recent years, layered van der Waals materials have emerged as promising hosts of ultra-bright quantum emitters²⁰. Integration of these light sources with dielectric and metallic waveguides has been achieved by placing flakes of the van der Waals hosts on top of the waveguides²¹⁻²³. However, in such a hybrid approach, the emitter couples only to the evanescent field of the cavity mode. Hence, spatial matching between the emitter and the electric field maximum is limited, and scattering losses are increased. A monolithic system, in which the photonic resonator hosts the quantum emitter is required for ideal on-chip devices.

Here, we design and fabricate optical cavities from hBN – a wide bandgap, hyperbolic van der Waals material^{20, 24, 25} that has recently attracted considerable attention as a promising host of ultra-bright, room-temperature quantum emitters^{20, 26-29}. In particular, we demonstrate two and one dimensional (2D) and (1D) photonic crystal cavities (PCCs) with optical Q -factors of up to 2,100. The fabricated cavities serve as building blocks for on-chip nanophotonic circuits based on hBN and for integration with active quantum systems. In contrast to mature semiconductors, nanofabrication protocols for van der Waals layered materials are not yet established, and the associated challenges are not fully understood. For example, it was unknown whether 2D stacked layers are sufficiently robust to endure nanofabrication processes without being destroyed. Also, undercutting techniques that are used to achieve suspended structures and bulk angle etch processes have not been applied successfully to these materials. In addition, a small refractive index of ~ 1.8 makes it hard to achieve a high refractive index contrast that is needed for efficient light confinement in the visible spectral range. In this work, we resolve these challenges by demonstrating the fabrication and iterative editing/tuning of suspended photonic cavities from the van der Waals material hBN using a combination of hBN exfoliation onto a trenched substrate, reactive ion etching (RIE) and single-step, direct-write electron beam induced chemical etching.

As a first step towards the nanofabrication of photonic cavities, we prepare thin layers of hBN by scotch tape exfoliation, as shown in Fig. 1a. The different colors indicate different thicknesses of hBN stacks. Due to the low refractive index of hBN, substrates cause severe optical losses. We therefore employed a substrate with pre-patterned trenches so that optical cavities can be fabricated in the suspended regions, as schematically depicted for the case of a 2D photonic crystal in Fig. 1b. Figure 1c is a scanning electron microscope (SEM) image of the suspended hBN showing the layered nature of hBN. Layers are held together by van der Waals forces and each 2D monolayer consists of alternating boron and nitrogen atoms arranged in a hexagonal pattern. The thicknesses of hBN flakes varies from a monolayer to a few hundred nm. Of these, only those with a thickness in the range of 200 nm - 500 nm were considered for fabrication since a single guided mode in the out-of-plane direction is generally preferred for photonic cavities.

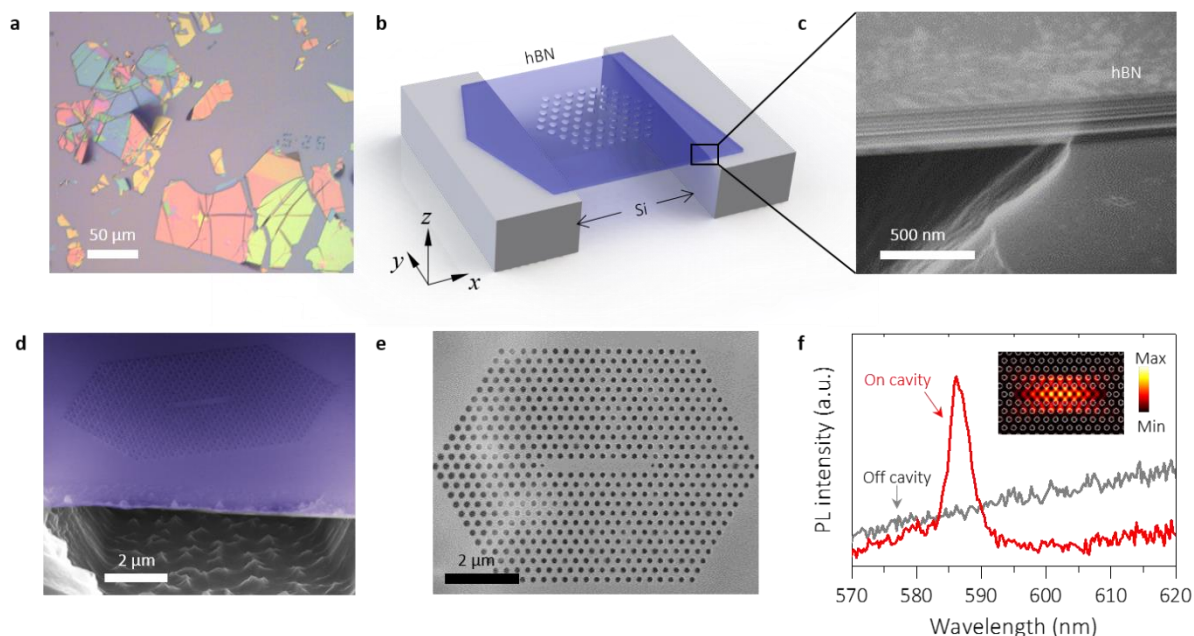


Figure 1 Free-standing hexagonal boron nitride 2D photonic crystal cavities. **a**, Optical microscope image of exfoliated hBN crystals on a silicon substrate. **b**, Schematic of a free-standing hBN cavity on a trenched silicon substrate. **c**, SEM image of the hBN showing the layered structure. **d**, false color SEM image (45°) of a free-standing hBN photonic crystal cavity fabricated using a combination of RIE and EBIE. **e**, Top view of a 2D photonic crystal cavity. **f**, Photoluminescence spectra with a laser exciting the cavity mode (red) compared to an off-cavity excitation (grey). The inset depicts the electric field intensity profile of the fundamental mode for the cavity calculated using 3D FDTD.

The first resonators that we show are 2D PCCs fabricated using a novel nanofabrication procedure that combines RIE with EBIE. Briefly, a tungsten layer that serves as a hard mask is deposited on top of hBN, followed by a thin layer of e-beam resist (polymethyl methacrylate (PMMA)). Using electron beam lithography, the 2D PCC pattern is written in the PMMA film followed by an RIE step in SF₆ gas, which transfers the 2D PCC pattern into the tungsten mask. The underlying hBN is then etched by material-selective EBIE using water vapor as a precursor gas³⁰, which results in nearly-straight sidewalls. Moreover, EBIE is a chemical process which does not rely on physical removal of atoms through knock-on processes that commonly occur in RIE and FIB techniques and cause substantial damage in the host crystal³¹. As a result, no post-processing (via annealing or wet-chemical treatment) is necessary after EBIE in order to observe and subsequently tune cavity modes, as is shown below. The EBIE process does not involve heavy ions (e.g. Ga) hence re-sputtering of ions and re-deposition of the etched material are absent. The process is explained further in the Supplementary Information.

Figure 1d shows a side view, false color SEM image of the 2D PCC fabricated in a suspended flake of hBN with nine holes missing in the center (L9 cavity). A top-view SEM image of the same cavity is shown in Fig. 1e. The geometries of the PCCs presented here were designed to have resonances in the visible spectral range³², where hBN quantum emitters are typically observed. To

achieve the desired resonances, we used a lattice constant (a) in the range of 240 nm – 300 nm, with an air hole radius in the photonic mirror region of $0.33a$ and two air holes at the end of the line defects with $0.22a$, shifted outwards by $0.22a$.

The fabricated cavities were analyzed optically using a confocal microscope setup at room temperature. A broadband hBN background emission is excited by a 532 nm continuous wave laser, and an objective lens with a numerical aperture of 0.9 is used for excitation and collection. A comparison of room temperature photoluminescence (PL) spectra measured by excitation of the cavity center with line defects (red) compared to excitation of an adjacent periodically patterned PCC area (grey) is shown in Fig. 1f. Excitation of the cavity yields an optical mode at 586.6 nm, whilst only a broad PL emission is observed when the laser spot is off the cavity. The electric field intensity profile of the measured mode is depicted in the inset, calculated using the 3D finite difference time domain (FDTD) method. By using a Lorentzian fit, a Q -factor of 160 is obtained. The observed Q -factor is relatively low, yet there are no other studies on 2D PCCs with similar or lower refractive index materials in the visible wavelength range. We note that, in practice, it is very challenging to open a photonic bandgap using a low refractive index material and a 2D cavity geometry.

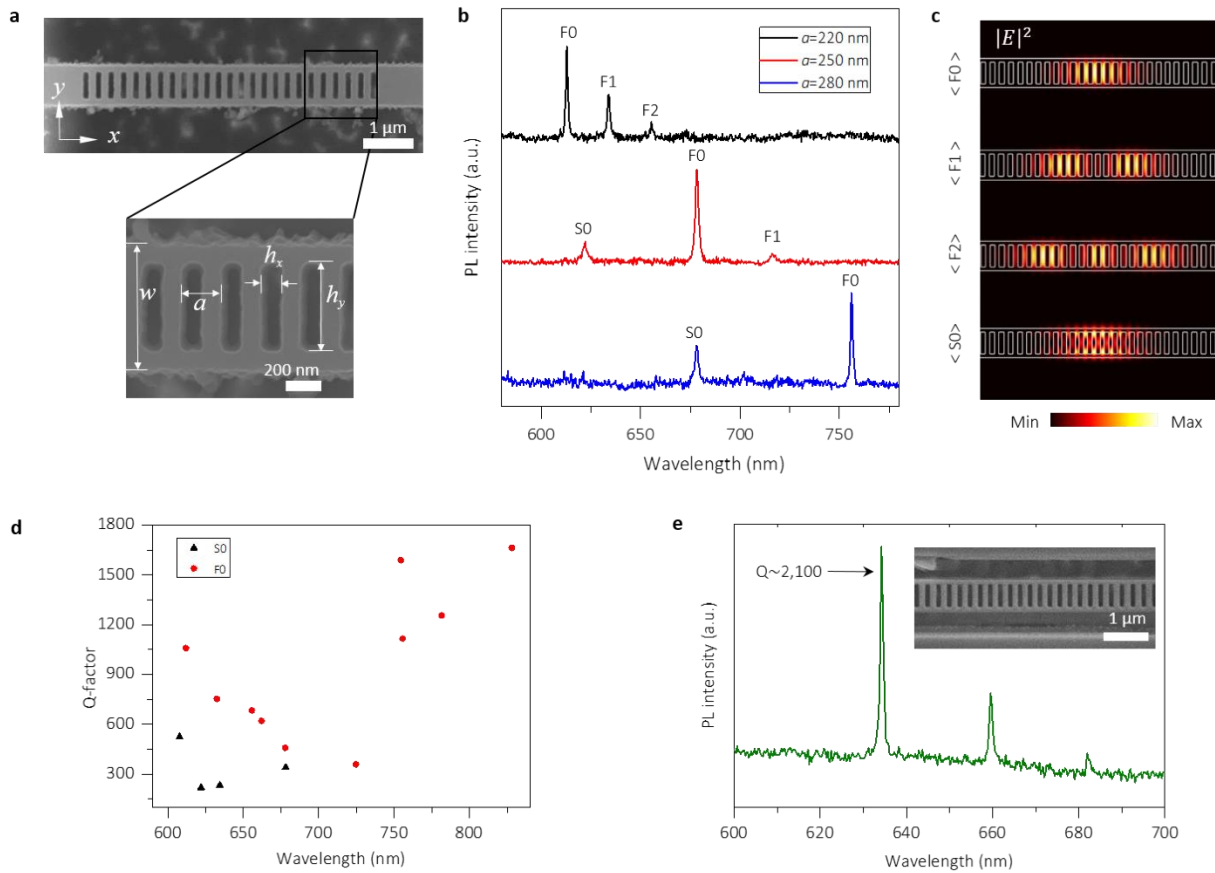


Figure 2 Optical analysis of one dimensional (1D) hBN photonic crystal cavities. **a**, SEM image of a 1D ladder PCC with 25 rectangular air holes and its magnified view, showing the geometrical parameters; width (w), lattice constant (a), air hole width (h_x) and air hole height (h_y). The cavity was fabricated using

a combination of RIE and EBIE. **b**, Photoluminescence spectra of different 1D ladder PCCs in the same hBN crystal with varying lattice constants of 220 nm (black), 250 nm (red), and 280 nm (blue), respectively. F0, F1, and F2 mark the position of the 0th, 1st, and 2nd order mode from the first dielectric band. S0 marks the position of the 0th order from the second dielectric band mode. **c**, 3D FDTD simulation result showing field profiles of the measured optical modes. **d**, Experimentally obtained Q -factors of various 1D PCCs fabricated from hBN. **e**, PL spectrum of a 1D cavity fabricated by focused ion beam milling, showing a high Q ($\sim 2,100$) mode in the visible spectral range. The inset is an SEM image of the cavity.

To achieve high Q cavities from low refractive index materials, it is more favorable to fabricate 1D ladder-type PCCs. Figure 2a shows representative SEM images of a 1D ladder PCC (beam width $w = 750$ nm) fabricated using the same combination of RIE and EBIE that was used to fabricate the cavity in Fig 1. The ladder contains 25 uniform-sized, rectangular air holes ($h_x = 150$ nm, $h_y = 550$ nm) with a lattice constant a of 250 nm (shown in Fig. 2a). The lattice constants of 19 air holes are modulated to form a photonic well at the center of the ladder structure with decreased lattice constants in the cavity region compared to the mirror region. Detailed information on the cavity design is given in Supplementary Information. Room temperature PL spectra acquired from three 1D ladder PCCs with lattice constants of 220 nm (black), 250 nm (red), and 280 nm (blue) are shown in Fig. 2b. The three cavities were fabricated in the same hBN flake that has a thickness of 280 nm. The 1D ladder cavity design has three confined resonant modes from the lowest energy photonic band as is observed in the PL spectrum obtained from the cavity with $a=220$ nm (Fig. 2b). These three modes are in good agreement with a spectrum obtained from FDTD simulation (Fig. S6c). The 0th order mode, also called the fundamental mode, from the first dielectric band (F0) is observed at 612.8 nm, while 1st order (F1) and 2nd order (F2) modes are observed at 633.9 nm and 655.5 nm, respectively. Here, ‘F’ designates that the modes originate from the ‘First’ dielectric band, and the numbers 0, 1 and 2 represent the number of nodes along the x-axis. These modes are all both TE modes and the dielectric modes, for which the electric field maximum is in the higher dielectric region (i.e. within the suspended hBN). Cavities with larger lattice constants have optical modes at longer wavelengths. For example, the measured F0 mode is at 678.4 nm for $a=250$ nm and 756.1 nm for $a=280$ nm (Fig. 2b). Higher energy modes, in this case the 0th order mode from the second dielectric band (S0), which are of interest for sensing applications due to their extended evanescent fields, are also observed for cavities with $a=250$ nm and $a=280$ nm. The electric field profiles of all observed modes, determined by 3D FDTD simulations, are depicted in Fig 2c. More details on simulation are included in Supplementary Information.

We fabricated and analyzed a number of cavities with a range of lattice constants. The Q -factor as a function of wavelength for both the first dielectric (F0, red circle) and the second dielectric (S0, black triangle) modes are summarized in Fig. 2d, including the cavity modes shown in Fig. 2b. Here among F0, F1 and F2, we only included F0 because modes with a lower number of nodes have higher Q -factors. The highest Q -factor measured from these cavities is 1700. Theoretical Q for a 1D photonic crystal cavity obtained using the 3D FDTD method with $a=250$ nm, $w=750$ nm, $h_x=130$ nm and $h_y=150$ nm corresponds to 53,000 and the resonant wavelength is 649.6 nm. The experimental Q is one order of magnitude lower mainly due to the roughness of sidewalls seen in Fig. 2a. We also note that higher Q -factors are expected from cavities with resonances at longer wavelengths because scattering caused by surface roughness is reduced. It is important to note that

this is the first report of such experimental Q values in a resonator made entirely from a layered van der Waals material.

To further investigate potential techniques for the fabrication of cavities from suspended hBN, we employed a focused ion beam. While FIB is an attractive option for direct milling of some materials, it causes damage within the crystal that must be recovered by annealing. However, the effectiveness of the annealing treatments varies substantially for different materials. For example, diamond cavities fabricated using a FIB have very low Q (< 800)³³ while yttrium orthosilicate (YSO) crystals show higher Q -factors of several thousands⁴. Figure 2e shows the PL spectrum of a cavity that was fabricated by FIB milling, and annealed (900 °C, Vacuum, 2 hrs) to recover FIB-induced damage. Additional details on fabrication of cavities by FIB milling is given in the Methods. Modes are observed at 634.2 nm (F0), 659.6 nm (F1), and 682.0 nm (F2), with a Q -factor as high as 2,100 for the F0 mode. We note that no modes were observed immediately after FIB fabrication, and the annealing step is required to remove residual damage. The inset is an SEM image of the cavity. A detailed comparison of cavities fabricated by both methods is given in the Supplementary and shows that for EBIE-fabricated cavities sidewalls within the air holes appear more vertical but rougher, while FIB-fabricated cavities show smooth sidewalls that are slanted. However, Raman analysis shows no evidence of damage directly after fabrication by EBIE, whilst residual damage is evident after FIB milling even after the annealing treatment that is required to observe modes. Hence, the Q -factor of the EBIE and FIB-fabricated cavities is likely limited by surface roughness and crystalline damage, respectively. The fact that EBIE processing does not require annealing is highly favorable for subsequent editing and iterative tuning of the cavities, as is discussed below.

The obtained cavities from hBN are on par with other bulk dielectric semiconductors that have much higher refractive indices in the visible wavelength range, as is summarized in Supplementary Information. Here, we focus on comparison with materials that are known to host quantum emitters in the visible range and have the potential for monolithic integration of emitter – cavity systems. These attributes make them particularly appealing to quantum photonic applications. Cavities fabricated using such materials have been shown to have the following Q -factors: YSO – $Q \sim 3,000$ at $\lambda = 596$ nm⁴, GaN – $Q \sim 5,200$ at $\lambda = 461$ nm³⁴, 4H SiC – 6,700 at $\lambda = 700$ nm³⁵ and diamond – $Q \sim 11,000$ at $\lambda = 734$ nm.

The Q -factors obtained from our hBN cavities are indeed promising for quantum photonic applications. Purcell enhancement of quantum emitters that are located optimally in the cavity field maximum is given by

$$F_p = \frac{3}{4\pi^2} \left(\frac{\lambda}{n}\right)^3 \frac{Q}{V},$$

where λ is the cavity resonance wavelength in free space, n is the refractive index at field anti node, and V is the mode volume. Using the ladder cavity, with $Q \sim 2,100$, a Purcell enhancement of ~ 110 can be achieved.

Next, we demonstrate that the optical modes of the fabricated cavities can be tuned deterministically by EBIE. Tuning is essential to match the resonance to the emission wavelength of the quantum emitter, particularly in the case of hBN where the emission wavelength varies

substantially and controlled fabrication of emitters with a given wavelength is yet to be demonstrated. In dielectric cavities, the resonant mode strongly depends on cavity parameters such as the width and thickness. Therefore, numerous methods exist to tune the cavity modes, such as thinning via oxidation or RIE, deposition of thin dielectric layers, or gas condensation. In this study, we demonstrate the use of EBIE to controllably tune individual cavities to shorter wavelengths without significant degradation of the Q -factor. As is shown schematically in Fig. 3a, the focused electron beam is guided along the outer sidewalls of a cavity, selectively etching these regions and reducing the width of the beam. In Fig. 3b the PL spectrum of a cavity is shown before tuning (black) with modes F0 and F1 at wavelengths of 745.2 nm and 771.7 nm, respectively. The reduced width of the 1D cavity results in a lower effective refractive index for the optical modes, which resulted in a blue shift of the cavity resonance by 2.4 nm (red) after the first tuning step. The same process was repeated again to demonstrate further tuning of an additional 4.2 nm (blue). It can be seen (Fig. 3c) that overall the Q -factor of the fundamental mode did not degrade significantly (a change of less than 10%) while that of the first 1st order mode increased. EBIE is therefore a reliable, robust method for tuning of PCC optical modes over a relatively wide spectral range. It does not cause substantial damage to the cavity and does not require subsequent RIE or deposition steps. The EBIE approach is therefore attractive for two reasons. First, being a localized, direct-write technique, it can be applied to individual cavities without affecting the modes or Q -factors of neighboring structures on the same chip. This is very challenging using deposition or RIE thinning techniques as they require additional masking steps and the low refractive index of hBN necessitates the use of suspended structures to realize high Q factors. Second, EBIE does not require any post-processing such as annealing that is needed to remove FIB-induced damage, or wet-etching used to etch regions processed by laser oxidation. As a result, the EBIE process can be applied iteratively to individual cavities on a single chip until the desired tuning is achieved.

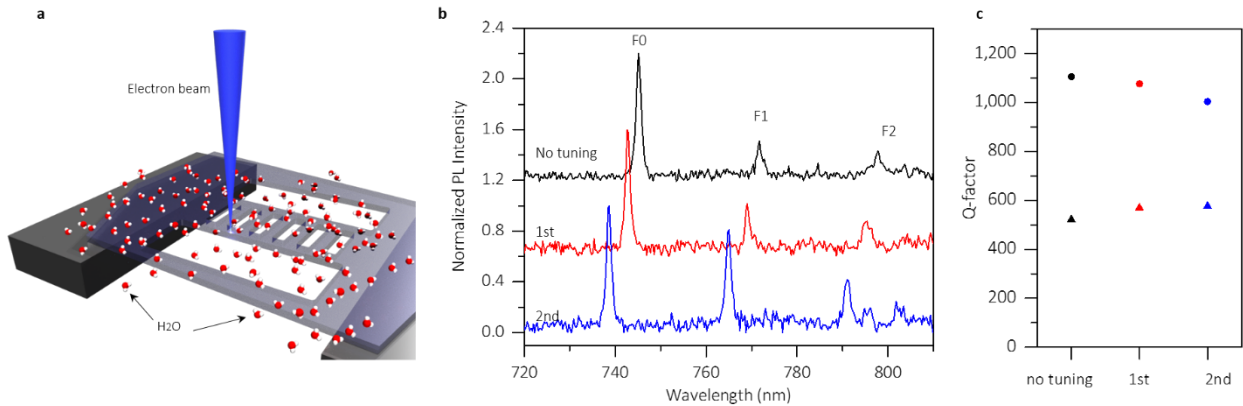


Figure 3 Tuning of a 1D nanobeam cavity using direct-write, maskless EBIE. a, Schematic of the etch process in which a focused electron beam (blue) is scanned along the outer sidewalls of the nanobeam cavity to induce the etch reaction in the presence of water molecules. **b,** Photoluminescence (PL) spectra of a 1D photonic cavity before tuning (black), and after the first (red) and second (blue) tuning steps were

performed by EBIE. c, Q -factor of the F0 (circles) and F1 (triangles) modes measured immediately after fabrication (black), and after the first (red), and second (blue) tuning steps.

Finally, we discuss the potential of integrating quantum emitters hosted by hBN with the fabricated PCCs. Coupling of an emitter to an optical mode requires both spatial and spectral overlap between the emitter and the cavity mode. The spatial overlap probability can be increased by deterministically creating single photon emitters in a non-destructive way with high precision. However, unlike the cases of other materials such as diamond and SiC, ion implantation and electron irradiation have not, to date, been shown to be reliable methods for the generation of quantum emitters in hBN. Furthermore, methods relying on strain field engineering or laser irradiation are not applicable in this case, as they will cause deformation of the suspended cavity and severe damage in the material, resulting in reduction of Q -factors. Hence, to create emitters in hBN, we employed an additional annealing step at 850°C after all the fabrication steps, as this method is known to generate single photon emitters²⁰ (albeit in random locations). To demonstrate the efficiency of this process, we compare the two regions shown in Fig. 4a - an unprocessed area on the left and a processed area that contains several nanobeams on the right. The corresponding PL map is shown in Fig. 4b. In the analyzed regions, we found a total of 13 single photon emitters, whose position are marked with yellow circles. Ten emitters are located directly in the fabricated cavities compared to 3 emitters found in the unpatterned area (Fig. 4c). The creation of extra emitters in the cavity-containing regions can be attributed to an increased surface area, creation of dangling bonds, activation of passivated defects, or chemical modification of sites that undergo partial chemical reactions during etching. Bright spots in the confocal map were analyzed spectrally and show clear narrowband zero phonon lines (ZPLs). In several cavities, we clearly observed spatial overlap between cavity modes and emitters, as is shown in Fig. 4d. The top plot (red) includes the ZPL at 710 nm from a color center and the optical mode of the cavity at 647.7 nm. The emitter is within the laser spot, which has a diameter of ~ 400 nm. Once the laser is spatially detuned from the emitter (bottom, blue curve), only the cavity mode remains, as expected. To confirm that the peak is indeed a single photon emitter, the emission lines are isolated by spectral filtering and the quantum nature is demonstrated using a Hanbury Brown and Twiss interferometer. The corresponding $g^2(\tau)$ curve with a zero delay time of $g^2(0)=0.26$ (measured without background subtraction) is shown in Fig. 4e, thus classifying it as a single photon source. We note that to demonstrate coupling between emitter and the optical mode, both spatial and spectral matching are required. However, despite the fact that the probability of spatial matching was increased by the processing steps used to fabricate the cavities (Fig. 4b and Fig. 4c), spectral matching was not observed because the emitters disappeared after an EBIE tuning step. This most likely happened because of the removal of material from the cavity edges during tuning, where the emitter was physically located. At this stage it has been difficult to find an emitter located in the middle of the dielectric mode of the cavity. Nevertheless, our method of tuning the cavity resonances, along with recent progress in fabrication of the emitters on demand^{28, 36, 37} is promising for eventual realization of coupled monolithic emitter-cavity systems made from hBN.

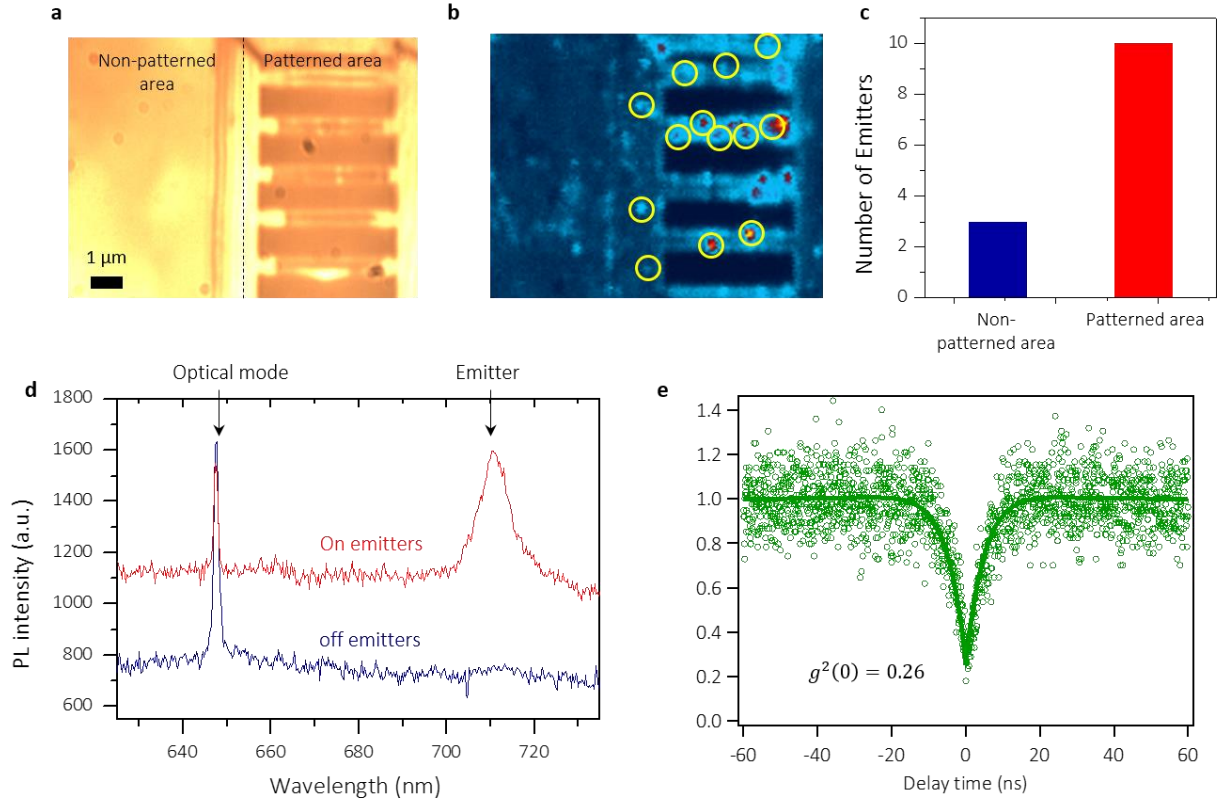


Figure 4 Generation of single photon emitters within the hBN cavities. **a**, optical microscope image of the analyzed area comparing an unprocessed site (left), with a processed site (right) that contains several 1D nanobeam cavities. **b**, corresponding Photoluminescence map of this region. Positions of quantum emitters are indicated by yellow circles **c**, a histogram summarizing the total number of single emitters found in unpatterned (blue) and patterned regions (red). **d**, PL spectra from two regions of the same cavity showing an optical mode only (blue) and the combination of an optical mode and an emitter (red). **e**, Measured $g^2(\tau)$ curve obtained from this emitter.

In summary, we have demonstrated for the first time the fabrication of photonic crystal cavities with Q -factors in excess of 2,000 from hBN, a promising van der Waals crystal. We employed both EBIE etching and FIB milling in protocols used to fabricate 1D and 2D PCCs. We also demonstrated a new technique to spectrally tune the optical mode of individual cavities using a maskless EBIE method. Finally, we showed that the cavity-patterned regions host a high density of quantum emitters, marking a first step towards monolithic integration of a hBN emitter-cavity system. Further developments in techniques for both deterministic fabrication of quantum emitters in hBN and resonant wavelength tuning will make weak and strong coupling experiments feasible. The present demonstration of hBN PCCs is already highly promising for applications in integrated on-chip quantum nanophotonics, optomechanics, cavity QED and quantum sensing experiments. Moreover, integration of hBN cavities with other 2D materials, may yield novel hybrid heterostructures for studies of light confinement at the nanoscale, and thus position 2D van der Waals systems as a unique platform in the field of integrated nanophotonics. Finally, the demonstrated ability to deterministically fabricate and tune hBN resonators will further expand its

applicability as a hyperbolic material for explorations of light confinement and polaritonics in the mid and near infrared spectral ranges.

Acknowledgements

The authors thank Dr T. Tran for assistance with Raman measurements and Dr C. Elbadawi for the assistance with EBIE. K.W. and T.T. acknowledge support from the Elemental Strategy Initiative conducted by the MEXT, Japan and JSPS KAKENHI, Grant Number JP15K21722. Financial support from the Australian Research council (via DP140102721), the Asian Office of Aerospace Research and Development grant FA2386-17-1-4064, the Office of Naval Research Global under grant number N62909-18-1-2025 are gratefully acknowledged.

Author contributions

S.K., I.A and M.T conceived the idea and designed experiments. J. E. F. developed the fabrication procedure for EBIE and tuning of cavities. S.K. performed the optical measurement and FDTD simulation. J.C. and M.S. provided cavities fabricated by FIB milling. K. W. and T. T. grew the hBN samples. J. B. assisted with EBIE experiments. D. T. prepared trenched silicon substrate. S.K., J. E. F., I.A. and M.T. co-wrote the manuscript.

References

1. Majumdar, A., Rundquist, A., Bajcsy, M. & Vučković, J. Cavity quantum electrodynamics with a single quantum dot coupled to a photonic molecule. *Phys. Rev. B* **86**, 045315 (2012).
2. Sekoguchi, H., Takahashi, Y., Asano, T. & Noda, S. Photonic crystal nanocavity with a Q-factor of ~9 million. *Opt. Express* **22**, 916-924 (2014).
3. Shen, Y., Harris, N.C., Skirlo, S., Prabhu, M., Baehr-Jones, T., Hochberg, M., Sun, X., Zhao, S., Larochelle, H., Englund, D. & Soljačić, M. Deep learning with coherent nanophotonic circuits. *Nat. Photonics* **11**, 441 (2017).
4. Zhong, T., Kindem, J.M., Miyazono, E. & Faraon, A. Nanophotonic coherent light-matter interfaces based on rare-earth-doped crystals. *Nat. Commun.* **6**, 8206 (2015).
5. Faraon, A., Barclay, P.E., Santori, C., Fu, K.M.C. & Beausoleil, R.G. Resonant enhancement of the zero-phonon emission from a colour centre in a diamond cavity. *Nat. Photonics* **5**, 301-305 (2011).
6. Mauranyapin, N.P., Madsen, L.S., Taylor, M.A., Waleed, M. & Bowen, W.P. Evanescent single-molecule biosensing with quantum-limited precision. *Nat. Photonics* **11**, 477 (2017).
7. Wu, S., Buckley, S., Schaibley, J.R., Feng, L., Yan, J., Mandrus, D.G., Hatami, F., Yao, W., Vuckovic, J., Majumdar, A. & Xu, X. Monolayer semiconductor nanocavity lasers with ultralow thresholds. *Nature* **520**, 69-72 (2015).
8. Lodahl, P., Mahmoodian, S. & Stobbe, S. Interfacing single photons and single quantum dots with photonic nanostructures. *Reviews of Modern Physics* **87**, 347-400 (2015).
9. O'Brien, J.L., Furusawa, A. & Vuckovic, J. Photonic quantum technologies. *Nat. Photonics* **3**, 687-695 (2009).
10. Kim, H., Bose, R., Shen, T.C., Solomon, G.S. & Waks, E. A quantum logic gate between a solid-state quantum bit and a photon. *Nat. Photonics*, 373-377 (2013).
11. Sipahigil, A., Evans, R.E., Sukachev, D.D., Burek, M.J., Borregaard, J., Bhaskar, M.K., Nguyen, C.T., Pacheco, J.L., Atikian, H.A., Meuwly, C., Camacho, R.M., Jelezko, F., Bielejec, E., Park, H., Lončar, M. & Lukin, M.D. An integrated diamond nanophotonics platform for quantum optical networks. *Science* (2016).

12. Aharonovich, I., Englund, D. & Toth, M. Solid-state single-photon emitters. *Nat. Photonics* **10**, 631-641 (2016).
13. He, X., Hartmann, N.F., Ma, X., Kim, Y., Ihly, R., Blackburn, J.L., Gao, W., Kono, J., Yomogida, Y., Hirano, A., Tanaka, T., Kataura, H., Htoon, H. & Doorn, S.K. Tunable room-temperature single-photon emission at telecom wavelengths from sp³ defects in carbon nanotubes. *Nat. Photonics* **11**, 577 (2017).
14. Chu, X.-L., Götzinger, S. & Sandoghdar, V. A single molecule as a high-fidelity photon gun for producing intensity-squeezed light. *Nat. Photonics* **11**, 58 (2016).
15. Senellart, P., Solomon, G. & White, A. High-performance semiconductor quantum-dot single-photon sources. *Nature Nanotech.* **12**, 1026 (2017).
16. Englund, D., Fattal, D., Waks, E., Solomon, G., Zhang, B., Nakaoka, T., Arakawa, Y., Yamamoto, Y. & Vuckovic, J. Controlling the spontaneous emission rate of single quantum dots in a two-dimensional photonic crystal. *Phys. Rev. Lett.* **95**, 013904 (2005).
17. Khasminskaya, S., Pyatkov, F., Słowik, K., Ferrari, S., Kahl, O., Kovalyuk, V., Rath, P., Vetter, A., Hennrich, F., Kappes, M.M., Gol'tsman, G., Korneev, A., Rockstuhl, C., Krupke, R. & Pernice, W.H.P. Fully integrated quantum photonic circuit with an electrically driven light source. *Nat. Photonics* **10**, 727 (2016).
18. Elshaari, A.W., Zadeh, I.E., Fognini, A., Reimer, M.E., Dalacu, D., Poole, P.J., Zwiller, V. & Jöns, K.D. On-chip single photon filtering and multiplexing in hybrid quantum photonic circuits. *Nat. Commun.* **8**, 379 (2017).
19. Davanco, M., Liu, J., Sapienza, L., Zhang, C.-Z., De Miranda Cardoso, J.V., Verma, V., Mirin, R., Nam, S.W., Liu, L. & Srinivasan, K. Heterogeneous integration for on-chip quantum photonic circuits with single quantum dot devices. *Nat. Commun.* **8**, 889 (2017).
20. Tran, T.T., Bray, K., Ford, M.J., Toth, M. & Aharonovich, I. Quantum emission from hexagonal boron nitride monolayers. *Nature Nanotech.* **11**, 37-41 (2016).
21. Tonndorf, P., Del Pozo-Zamudio, O., Gruhler, N., Kern, J., Schmidt, R., Dmitriev, A.I., Bakhtinov, A.P., Tartakovskii, A.I., Pernice, W., Michaelis de Vasconcellos, S. & Bratschitsch, R. On-Chip Waveguide Coupling of a Layered Semiconductor Single-Photon Source. *Nano Lett.* **17**, 5446-5451 (2017).
22. Cai, T., Dutta, S., Aghaeimeibodi, S., Yang, Z., Nah, S., Fourkas, J.T. & Waks, E. Coupling Emission from Single Localized Defects in Two-Dimensional Semiconductor to Surface Plasmon Polaritons. *Nano Lett.* **17**, 6564-6568 (2017).
23. Schell, A.W., Takashima, H., Tran, T.T., Aharonovich, I. & Takeuchi, S. Coupling Quantum Emitters in 2D Materials with Tapered Fibers. *ACS Photonics* **4**, 761-767 (2017).
24. Cassabois, G., Valvin, P. & Gil, B. Hexagonal boron nitride is an indirect bandgap semiconductor. *Nat. Photonics* **10**, 262 (2016).
25. Giles, A.J., Dai, S., Vurgaftman, I., Hoffman, T., Liu, S., Lindsay, L., Ellis, C.T., Assefa, N., Chatzakis, I., Reinecke, T.L., Tischler, J.G., Fogler, M.M., Edgar, J.H., Basov, D.N. & Caldwell, J.D. Ultralow-loss polaritons in isotopically pure boron nitride. *Nature Mater.* (2017).
26. Shotan, Z., Jayakumar, H., Considine, C.R., Mackoite, M., Fedder, H., Wrachtrup, J., Alkauskas, A., Doherty, M.W., Menon, V.M. & Meriles, C.A. Photoinduced Modification of Single-Photon Emitters in Hexagonal Boron Nitride. *ACS Photonics* **3**, 2490-2496 (2016).
27. Jungwirth, N.R., Calderon, B., Ji, Y., Spencer, M.G., Flatt, M.E. & Fuchs, G.D. Temperature Dependence of Wavelength Selectable Zero-Phonon Emission from Single Defects in Hexagonal Boron Nitride. *Nano Lett.* **16**, 6052-6057 (2016).
28. Chejanovsky, N., Rezai, M., Paolucci, F., Kim, Y., Rendler, T., Rouabeh, W., F?varo De Oliveira, F., Herlinger, P., Denisenko, A., Yang, S., Gerhardt, I., Finkler, A., Smet, J.H. & Wrachtrup, J.r.

- Structural Attributes and Photodynamics of Visible Spectrum Quantum Emitters in Hexagonal Boron Nitride. *Nano Lett.* **16**, 7037-7045 (2016).
29. Bourrellier, R., Meuret, S., Tararan, A., Stéphan, O., Kociak, M., Tizei, L.H.G. & Zobelli, A. Bright UV Single Photon Emission at Point Defects in h-BN. *Nano Lett.* **16**, 4317-4321 (2016).
 30. Elbadawi, C., Tran, T.T., Kolibal, M., Sikola, T., Scott, J., Cai, Q., Li, L.H., Taniguchi, T., Watanabe, K., Toth, M., Aharonovich, I. & Lobo, C. Electron beam directed etching of hexagonal boron nitride. *Nanoscale* **8**, 16182-16186 (2016).
 31. Utke, I., Moshkalev, S. & Russell, P. Nanofabrication Using Focused Ion and Electron Beams. (Oxford University Press, New York, 2012).
 32. Kim, S., Toth, M. & Aharonovich, I. Design of photonic microcavities in hexagonal boron nitride. *Beilstein Journal of Nanotechnology* **9**, 102-108 (2018).
 33. Riedrich-Moller, J., Kipfstuhl, L., Hepp, C., Neu, E., Pauly, C., Mucklich, F., Baur, A., Wandt, M., Wolff, S., Fischer, M., Gsell, S., Schreck, M. & Becher, C. One- and two-dimensional photonic crystal microcavities in single crystal diamond. *Nature Nanotech.* **7**, 69-74 (2012).
 34. Rousseau, I., Sánchez-Arribas, I., Shojiki, K., Carlin, J.-F., Butté, R. & Grandjean, N. Quantification of scattering loss of III-nitride photonic crystal cavities in the blue spectral range. *Phys. Rev. B* **95**, 125313 (2017).
 35. Bracher, D.O. & Hu, E.L. Fabrication of High-Q Nanobeam Photonic Crystals in Epitaxially Grown 4H-SiC. *Nano Lett.* **15**, 6202-6207 (2015).
 36. Proscia, N.V., Shotan, Z., Jayakumar, H., Reddy, P., Dollar, M., Alkauskas, A., Doherty, M.W., Meriles, C.A. & Menon, V.M. Near-deterministic activation of room temperature quantum emitters in hexagonal boron nitride. *arXiv:1712.01352* (2018).
 37. Xu, Z.-Q., Elbadawi, C., Tran, T.T., Kianinia, M., Hoffman, T.B., Edgar, J.H., Toth, M. & Aharonovich, I. Atomic Engineering of Single Photon Sources in 2D Boron Nitride Zai-Quan. *arXiv preprint arXiv:1704.05154* (2017).